



Titre: Femtosecond laser direct-writing of high quality first-order Bragg gratings with arbitrary complex apodization by phase modulation
Title:

Auteurs: Anthony Roberge, Sébastien Loranger, Jean-Sébastien Boisvert, Frédéric Monet, & Raman Kashyap
Authors:

Date: 2022

Type: Article de revue / Article

Référence: Roberge, A., Loranger, S., Boisvert, J.-S., Monet, F., & Kashyap, R. (2022). Femtosecond laser direct-writing of high quality first-order Bragg gratings with arbitrary complex apodization by phase modulation. Optics Express, 30(17), 30405-30419. <https://doi.org/10.1364/oe.465331>
Citation:

Document en libre accès dans PolyPublie

Open Access document in PolyPublie

URL de PolyPublie: <https://publications.polymtl.ca/54317/>
PolyPublie URL:

Version: Version officielle de l'éditeur / Published version
Révisé par les pairs / Refereed

Conditions d'utilisation: Optica Open Access Publishing Agreement
Terms of Use:

Document publié chez l'éditeur officiel

Document issued by the official publisher

Titre de la revue: Optics Express (vol. 30, no. 17)
Journal Title:

Maison d'édition: Optica Publishing Group
Publisher:

URL officiel: <https://doi.org/10.1364/oe.465331>
Official URL:

Mention légale: © 2022 Optica Publishing Group under the terms of the Open Access Publishing Agreement. Users may use, reuse, and build upon the article, or use the article for text or data mining, so long as such uses are for noncommercial purposes and appropriate attribution is maintained. All other rights are reserved.
Legal notice:



Femtosecond laser direct-writing of high quality first-order Bragg gratings with arbitrary complex apodization by phase modulation

ANTHONY ROBERGE,^{1,*}  SÉBASTIEN LORANGER,² 
JEAN-SÉBASTIEN BOISVERT,¹ FRÉDÉRIC MONET,¹ AND RAMAN
KASHYAP^{1,2}

¹Department of Engineering Physics, Polytechnique Montreal, 2500 Chemin de Polytechnique, Montréal H3T 1J4, Canada

²Department of Electrical Engineering, Polytechnique Montreal, 2500 Chemin de Polytechnique, Montréal H3T 1J4, Canada

*anthony.roberge@polymtl.ca

Abstract: Femtosecond laser direct-writing is an attractive technique to fabricate fiber Bragg gratings and to achieve through-the-coating inscription. In this article, we report the direct inscription of high-quality first-order gratings in optical fiber, without the use of an index-matching medium. A new alignment technique based on the inscription of weak probe gratings is used to track the relative position between the focal spot and fiber core. A simple and flexible method to precisely control the position of each grating plane is also presented. With this method, periodic phase modulation of grating structures is achieved and used to inscribe arbitrary apodization and phase profiles. It is shown that a burst of multiple laser pulses used to inscribe each grating plane leads to a significant increase in the grating strength, while maintaining low insertion loss, critical for many applications.

© 2022 Optica Publishing Group under the terms of the [Optica Open Access Publishing Agreement](#)

1. Introduction

With their abilities to photo-induce strong refractive index modification (RIM) in a wide variety of materials and through the coating of fibers, femtosecond (FS) lasers have enabled the fabrication of fiber Bragg grating (FBG) with an extensive number of functionalities [1–3]. The phase mask [4] and direct-writing method [5] are the two most widespread techniques to inscribe FBG using FS lasers. While the phase mask technique is excellent for its simplicity, stability, reproducibility, spectral quality, and for mass production, it does not provide the same flexibility attributed to direct-writing methods [1,6]. In particular, the requirement of a custom apodized phase mask [7,8] severely limits the potential to quickly prototype various complex grating design, as they can be expensive, difficult to make and are limited in length.

Instead of being imprinted in the phase mask, the grating parameters such as the Bragg wavelength, chirp, length, apodization profile or cladding mode coupling can be adjusted and reconfigured easily using direct inscription. However, several improvements are still needed to enhance the performance of the current fabrication methods. For instance, due to the small size of the laser focal cross-section, a highly accurate alignment between the focal spot and the fiber core is of crucial importance to ensure a good overlap between the RIM and the mode field [6,9]. Deviation from the core center can significantly reduce the coupling coefficient (κ), increase coupling to higher order modes and increase photo-induced birefringence [6,9–12]. Alignment methods based on imaging the fiber core [13] can achieve good results, but often require some extra calibration steps for different types of fiber, which can yield variable result. Another attractive feature of direct-writing methods is their potential to fabricate any user defined structure. Even though many apodization [14–16] and phase control [14,17,18] schemes have

been demonstrated, the ability to control amplitude and phase is not trivial, making it difficult to achieve high quality FBGs with true arbitrary complex profiles. Furthermore, despite the fact that FS direct-writing of first-order gratings have been demonstrated [6,19–21], achieving high κ together with low insertion loss, low polarization dependency and low coupling to cladding mode has been difficult because of the tradeoff between pulse energy, grating visibility and scatter loss. To overcome these difficulties and the requirement of a sub-micrometer RIM, many have resorted to writing high-order gratings [14,16,19,22] with larger periods.

The aim of this article is to present a different approach that can be implemented with FS direct-writing techniques to improve the ability to fabricate high-quality first-order gratings with arbitrary complex apodization and phase profile. First, a novel alignment technique is proposed and demonstrated with the inscription of multiple weak probe gratings to map the position of the fiber core with respect to the laser focus. Then, we show that a burst of multiples pulses can be used to significantly increase the grating strength while maintaining low insertion loss and high spectral quality. Finally, we present how apodization by periodic phase modulation [23] can be used to control the amplitude of the grating with high precision and with a spatial resolution down to a few grating periods. To precisely control the position of each grating plane, a simple and efficient phase control strategy based on position synchronized output (PSO) tracking [24] is demonstrated.

2. Writing scheme

2.1. Experimental setup

The experimental setup used to fabricate FBGs by our direct-writing method is shown in Fig. 1. A plane-by-plane (PI-b-PI) writing scheme [6] was chosen, as it allows for a larger overlap between the RIM and the mode field, which helps to achieve lower broadband losses, smaller coupling to cladding modes and higher grating strength [6,9,25] compared to the point-by-point (PbP) [5] or line-by-line (LbL) [26] techniques.

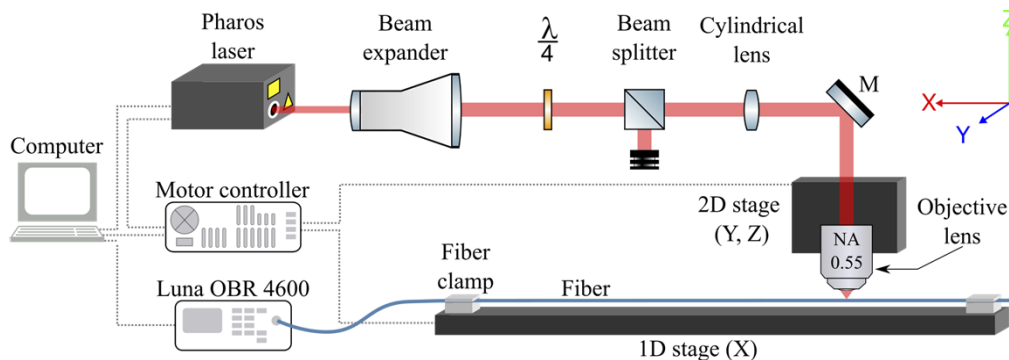


Fig. 1. Experimental setup for direct-writing of FS FBGs. The beam passes through a beam expander to match the objective NA. A quarter waveplate ($\lambda/4$) and beam splitter are used to adjust the power. A cylindrical lens with a focal length of 1 m is placed before the objective (NA = 0.55) to shape the focal spot into a plane. The fiber is held onto a 1D Aerotech stage with the help of clamps. The fabrication process is monitored using a Luna 4600 optical backscatter reflectometer (OBR). The polarization of the laser is perpendicular to the longitudinal axis (x).

An 8 W Pharos laser from Light Conversion is used. The laser, operating at a wavelength of 1030 nm, has a pulse duration of 250 fs and repetition rate of 606 kHz which can be tuned with a pulse picker. The beam is focused through a plano-convex aspheric lens (Newport, NA = 0.55)

that is mounted on a 2D air-bearing Aerotech translation stage. The fiber is clamped on a high-precision 1D air-bearing Aerotech stage which has a travel length of 1 m controlled by an interferometric laser-based encoder [27]. The inscriptions are performed over free-standing fibers and without index-matching oil. If needed, the coating can be removed using methylene chloride, followed by cleaning the fiber. A small tension (~ 150 g) is applied to the fiber to minimize its sag. A 1 m focal length cylindrical lens is placed before the objective to shape the focal spot into a planar stripe [6]. Much like the PbP approach, each plane is written in a single step, making the scheme faster than the LbL method [21,26].

A multi-pulse approach is used, where each grating plane is formed with a burst of lower-energy pulses instead of a single high-energy pulse [28–31]. The advantages of such method will be described in section 4.2. The writing speed is adjusted relative to the repetition rate and number of pulses per grating plane. It is set to keep the distance travelled by the stage during a single burst to a fraction of the grating period. Speeds of 0.03–0.3 mm/s are normally used.

All the FBGs reported in this work are written in the first order.

2.2. Phase control strategy

In order to fabricate gratings with complex spectral profiles, a precise control of the grating phase is required. For example, the method of apodization presented in this paper, i.e. phase modulation, requires a precise control over the position of each grating plane. For FS direct-writing many phase control methods have been proposed, each of them having their own limitations. For instance, controlling the speed/acceleration profile of the stage [17,32] is limited to continuous and slow-varying chirps, modulation of the laser repetition rate [6,14] requires additional electronics and is also limited in terms of phase control, and the stop-and-go scheme used with LbL method [18] is slow compared to PbP.

To address these limitations, the position synchronized output (PSO) feature of the motor controller is used to synchronize the triggering of a laser pulse (or burst of pulses for a multi-pulse approach) with the position of the stage, as it moves at constant speed [24]. The PSO functionality is provided with most of Aerotech motion controllers. It uses direct feedback from the encoder of the stage to track the position of multiple axis, and it sends trigger signals very precisely at specified positions, allowing precise control of the phase which is critical for the apodization method described in this work. This enables the fabrication of uniform or arbitrary complex grating structures.

3. Fiber core position mapping

3.1. Alignment principle

A common technique for fiber alignment is to image the core of the fiber with a camera system [6,9,13,33]. With proper calibration and optical alignment, both the camera and laser can share the same optical path and focal point, but the ability to visualize the core ultimately depends on the focusing conditions and the fiber properties such as the core-cladding refractive index difference, the core size, the type of coating, etc. Using a V groove with a coverslip [17,34,35], a drawing ferrule [3,14], and index-matching oil can help to maintain a proper alignment and to visualize the core, but these methods require additional custom components, and oil immersion can degrade the fiber and requires the fiber to be cleaned after the inscription.

The indirect alignment technique proposed here is based on optimizing the position where the laser focal spot maximizes the coupling coefficient κ of a grating. To do so, a cascade of small uniform FBGs, called alignment probes, are written at various transverse displacements around the core of the fiber, as shown in Fig. 2-(A). The probes are evenly spaced along the x-axis, within a characterization section which is assumed to be relatively uniform. The strength of the probes is orders of magnitudes weaker than the final intended grating, hence they do not affect its

spectral response nor degrade the fiber. The relative strength of each probe, proportional to κ , is then measured using an optical frequency domain reflectometry (OFDR) system which can not only detect very weak scatter events, but also discriminate their positions along the fiber [36]. As the exposure is equal for all probes, variation in probe signal is proportional to the overlap between the focal spot and the mode field. Therefore, this signal should vary approximately as a Gaussian function of the transverse displacement [37].

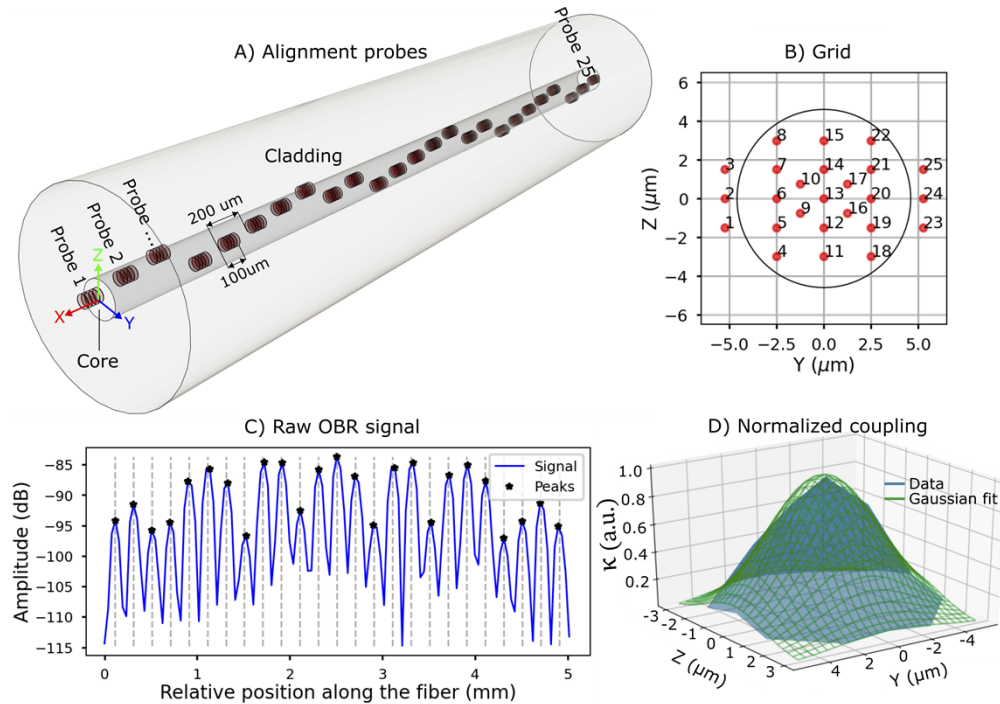


Fig. 2. A) Illustration of the alignment probes, consisting of several uniform FBGs. Each probe has a length of 0.1 mm and are spaced 0.1 mm from each other. B) Grid that represent the position of each probe in the transverse plane (y - z) of the fiber. The circle depicts the mode field diameter of an SMF-28 fiber. The numbers represent the longitudinal order (along x) in which they are inscribed. C) Spatial impulse response acquired by the OBR for one iteration of the mapping process (25 probes). Each peak corresponds to one probe for which the amplitude is proportional to κ . D) The same data can be rearranged into a 2D map representing the normalized peak amplitude of each probe in the iteration, for which a Gaussian fit can be applied to find the center point. Each iteration takes about 20 seconds, repeated every 5 mm.

Inscription of alignment probes in a single characterization section is shown schematically in Fig. 2-(A), where 25 alignment probes are written near what is thought to be the center of the fiber. The probes are 100 μm long and are separated from each other by 100 μm , resulting in a mapping resolution along the longitudinal axis of the fiber of 5 mm. To ensure uniform RIM and avoid a slight effective index modulation, exposure is kept constant even between the probes. Probes are switched ON/OFF by apodization, which is explained later in the article. The relative position of each probe forms a 2D grid which cover the whole core of the fiber, as shown in Fig. 2-(B). The spatial measurement of the strength of the probe FBGs by OFDR is shown in Fig. 2-(C). The peak amplitude of each probe is then rearranged in 2D where a Gaussian curve can be fitted to find the position of best alignment, as shown in Fig. 2-(D). This procedure is then

repeated automatically with the help of an in-house software until the whole region of interest of the fiber is mapped. Note that the initial position of the focal spot must be within $\sim 10 \mu\text{m}$ from the core position to get a signal. It can be found by inscribing trial probes over a larger area than the grid of Fig. 2-(B).

3.2. Mapping result

Using the alignment procedure and experimental setup presented in Fig. 2, the fiber core position of both an uncoated and a polyimide coated SMF-28 fiber were mapped over a length of 500 mm. Both fibers were free standing in air (no index-matching medium). Figure 3 shows the alignment position, where a low-pass filter is used to remove the noise in the position signal.

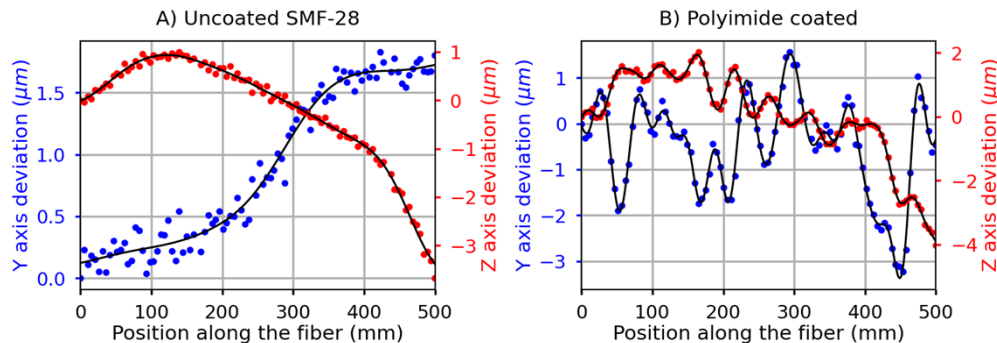


Fig. 3. Mapping of the core position of two different fibers. The mapping is presented as a relative deviation from the initial position of the focusing objective. The raw data is filtered with a low-pass filter. A) Uncoated SMF-28. B) Polyimide coated SMF-28 fiber.

In the case of an uncoated fiber (Fig. 3-(A)), the geometry of the fiber is usually found to be very uniform along its length, and the core position varies smoothly with respect to the laser focal spot. The core can be tracked with sub-micrometer precision, as the residual standard deviation of the signal noise is below $0.1 \mu\text{m}$ for both the Y and Z axis.

This high level of precision becomes critically useful with a coated fiber where strong oscillations of a few μm can be observed (Fig. 3-(B)) as a function of the position. These are attributed to the inhomogeneous nature of the polymer coating, which is prone to significant thickness and curvature fluctuations along the fiber, thus creating optical aberrations of the focal spot shape and position. This is especially true in an air-based system, where the refractive index mismatch is large. Nevertheless, it is still possible to track the slow fluctuations of the core position of coated fibers with high accuracy. However, it should be noted that this tracking does not correct for focal spot shape distortion, which adds amplitude and phase noise to the grating while writing through a polyimide coated fiber, making it more difficult to inscribe high-quality grating over long lengths.

4. Grating fabrication

4.1. Uniform grating

To demonstrate the performance of our writing scheme, we start by showing the reflection and transmission spectra of uniform FBGs in Fig. 4. Two first-order gratings were inscribed in both an uncoated SMF-28 (Fig. 4-(A)) and a polyimide coated SMF-28 fiber (Fig. 4-(B)). They had a length of 10 mm and a central wavelength of 1572 nm. The grating fabricated in the uncoated SMF-28 was written at a speed of $60 \mu\text{m/s}$, using a laser repetition rate of 606 kHz, a pulse energy of 270 nJ (measured before the objective) and with a burst of 150 pulses/plane. The

grating made through the polyimide coating was written at a speed of $15 \mu\text{m/s}$, a laser repetition rate of 60.6 kHz , a pulse energy of 290 nJ and with a burst of 50 pulses/plane . When writing through the coating, a slower repetition rate is used to prevent heat accumulation effects, which degrade the coating and spectral response. The dashed lines show the theoretical response for a uniform grating, fitted to the data.

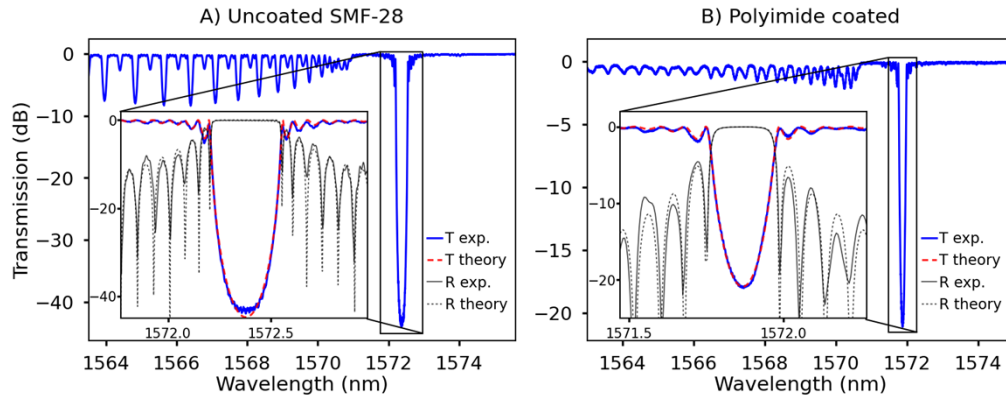


Fig. 4. Experimental (Exp.) and theoretical (dashed lines) spectra of the transmission and reflection of 10 mm long FBGs made in an uncoated (bare) SMF-28 fiber (A) and a polyimide coated fiber (B), the latter being written at the maximum energy without damage to the coating.

The FBG spectra shown in Fig. 4 are strong ($\kappa L > 3$), with a very symmetric and high-quality spectral response, as can be seen from the excellent agreement between the experimental data and the theoretical fits to the spectra. The resulting coupling coefficients κ for both FBGs, calculated from their peak reflectivity [38], are respectively, 575 m^{-1} and 308 m^{-1} . Out-of-band insertion loss of $< 0.1 \text{ dB}$ is measured for both the uncoated and coated grating. A more detailed characterization of the insertion loss is given in the next section. As seen from Fig. 4, strong coupling to cladding modes can be observed. This is expected as the laser focusing condition used in this work produces an asymmetrical RIM that does not cover the entire core cross section [9]. However, we believe coupling to cladding mode can be further decreased by modifying the focal spot geometry with additional beam shaping techniques [9,22,39–41].

Figure 5 shows the polarization dependence of a 10 mm FBG with a transmission dip of -25 dB , made under similar conditions. The birefringence (Δn_B) is measured at $6.2 \times 10^{-6} \text{ RIU}$, which is near the intrinsic birefringence of SMF-28 (10^{-6} RIU), and therefore at the limit of our measuring capability. This confirms low polarization dependency of the PI-b-PI scheme.

4.2. Single-pulse vs. multi-pulse approach

Multi-pulse approach has been widely used in the fabrication of Bragg gratings, waveguides, and the combination the two [28–31]. It provides control over the physical size and the overlap of the RIM, the deposited energy, and cumulative effect allows for a smoother RIM, with stronger refractive index change and lower loss, while keeping the pulse energy well below the damage threshold.

To understand how the multi-pulse approach affects the refractive index change, κ was measured as a function of the pulse energy and for different number of laser pulses per grating plane. This was done by writing several FBGs in both an uncoated SMF-28 fiber and a polyimide coated fiber, the results of which are shown in Fig. 6-(A) and Fig. 6-(B). In all cases, κ grows with the pulse energy up to a certain threshold (indicated with dashed lines) where a local maximum can be observed. This is followed by a local minimum (or small plateau as shown in the inset of

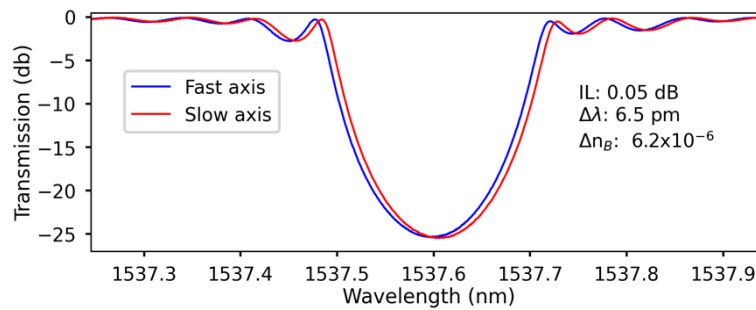


Fig. 5. Polarization dependency for a uniform FBG made with the PI-b-PI scheme and a burst of 150 pulses/plane.

Fig. 6-(A)). This type of transition was also observed in [30], but the exact mechanism responsible for it is still being investigated. When writing with pulse energies below the transition, high spectral quality and low insertion loss are observed, while writing above this transition yields lossy grating (several dB/cm), as shown in Fig. 6-(C)-D, with a deterioration of the spectral response (See Fig. S1 in the supplementary material). We believe this threshold could be caused by a transition from type-I to type-II structures, usually associated with optical damage and high scattering loss of the sample [30].

To arrive at a better understanding of the losses induced by this writing scheme, Fig. 6-(C) and Fig. 6-(D) show the out-of-band insertion loss measured for FBGs written at pulse energies above and below the transition and for different number of laser pulses per grating plane. This was measured by subtracting a reference transmission spectrum from the sample spectrum and by evaluating the average loss for wavelengths above the Bragg wavelength. In both types of fiber, low insertion losses < 0.1 dB/cm were measured for pulse energies below the transition, which is in good agreement with the loss measured in [6], even for high κ value.

Most interestingly, this experiment suggests that the multi-pulse approach can increase the maximum κ value at which low-loss gratings can be inscribed compared to what is possible with a single pulse. With lower energy pulses, the focal region where the light intensity is just above threshold for RIM is reduced. Unfortunately, this also reduces the Fourier component of the fundamental period. With each additional pulse, the RIM region expands through nonlinear multiphoton absorption, as well as from the total fluence, increasing the κ value. This improvement emerges from the cumulative effect of multiple pulses. On the other hand, a single high intensity pulse being closer to the damage threshold of the fiber is more likely to lead to Type-II grating very quickly. Further studies are in progress to clarify the physical mechanisms contributing to this improvement and will be reported on in a future publication.

When writing through a polyimide coating, we note that it was not possible to obtain a κ value as strong as for the uncoated fiber before observing a degradation of the spectral response and higher losses. A different focusing arrangement may of course, be used to optimize the RIM cross-section or make a better overlap to begin with using a single pulse, and hence increase the kappa values even more. This could be achieved with advanced beam shaping techniques [9,22,39–41].

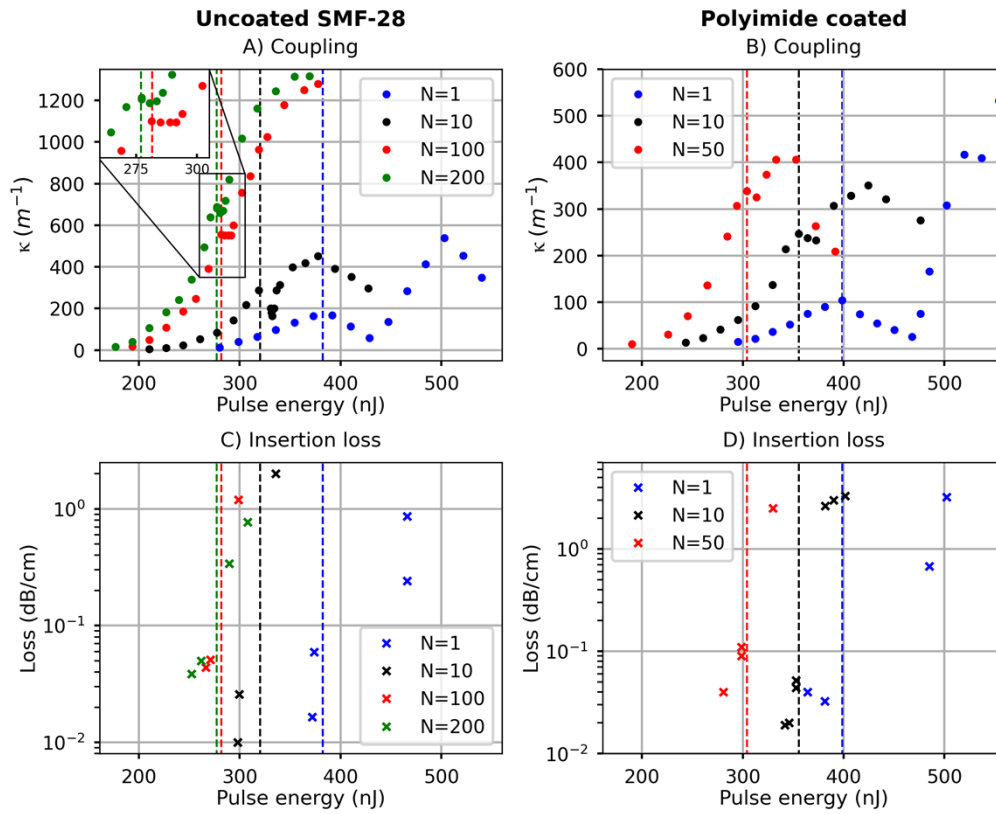


Fig. 6. A) and B) Coupling coefficient for FBGs inscribed as a function of the pulse energy and the number of pulses per grating plane (N). The dashed lines indicate the pulse energy threshold where a transition between two writing regimes can be observed. C) and D) Out-of-band insertion loss for FBGs inscribed above and below the transition pulse energy threshold as indicated by the dashed lines. The study was made using both an uncoated SMF-28 fiber (A and C), and a polyimide coated SMF-28 fiber (B and D).

5. Apodization by phase modulation

5.1. Apodization

For FS direct-writing, various amplitude apodization techniques were previously proposed. For instance, $\kappa(x)$ can be controlled by varying the transverse position of the RIM [37,42] or by pulse energy regulation [15,43]. These ideas were also implemented with the LbL method [16,18], where apodization is achieved by adjusting the writing velocity, length, or transverse position of each line. Despite the progress, all these techniques induce a spatial variation in the average RIM which causes asymmetric non-linear chirp. Ideally, apodization should be performed by keeping the average RIM constant. This can be achieved by controlling the grating visibility instead of the exposure or RIM position.

Towards that end, the technique of apodization by phase modulation [23,44,45] is proposed and applied to our direct-writing scheme. By simply modulating the phase of the grating, this technique enables apodization with constant laser power and exposure, hence maintaining a constant average RIM and mitigating the challenge of handling highly non-linear induced RIM vs laser power [15,18]. Apodization by phase modulation is achieved by incorporating an additional periodic function with a slowly varying amplitude to the grating phase. Any periodic function can

be used [23], but in this article, a sinusoidal function is chosen. The refractive index modulation of the grating can be expressed as:

$$\Delta n(x) = \overline{\Delta n}(x) \left(1 + v(x) \cos \left(\frac{2\pi x}{\Lambda_g} + \phi_g(x) + A(x) \sin \left(\frac{2\pi x}{\Lambda_\phi} \right) \right) \right), \quad (1)$$

where x is the position along the fiber, Λ_g is the grating period, $\overline{\Delta n}$ is the average refractive index change over Λ_g , v is the visibility, ϕ_g is the grating phase and $A(x) \sin(2\pi x/\Lambda_\phi)$ is the additional phase modulation function of period Λ_ϕ and amplitude profile, $A(x)$. Traditionally, apodization is achieved by controlling $\overline{\Delta n}(x)$ or $v(x)$ to modify the grating envelope. In a phase modulation scheme, both are kept constant, and the profile of $A(x)$ determines the grating apodization. By expanding Eq. (1) in a Fourier series, the refractive index modulation becomes [45]:

$$\Delta n(x) = \overline{\Delta n} \left(1 + v \sum_{m=-\infty}^{\infty} J_m(A(x)) \cos \left(\frac{2\pi x}{\Lambda_g} + \phi_g(x) + m \frac{2\pi x}{\Lambda_\phi} \right) \right), \quad (2)$$

where J_m is the m^{th} Fourier component, defined by a Bessel function of the same order. The 0^{th} Fourier component ($m = 0$) is related to the main Bragg resonance, and the $\pm m^{\text{th}}$ are optical superlattice sidebands due to the periodic modulation. To ensure that these sidebands are outside of the optical operation band of the FBG, a sufficiently small period Λ_ϕ should be chosen [23]. Considering only the 0^{th} component of Eq. (2) $J_0(A(x))$ acts as the envelope function of the grating, i.e. similar to the visibility. Hence, $A(x)$ is related to the normalized target apodization profile $|\kappa_n(x)|$ by an inverse Bessel function:

$$A(x) = J_0^{-1}(|\kappa_n(x)|). \quad (3)$$

Note that for the following demonstration, the grating profile is represented with a complex coupling coefficient $\kappa_n(x)$, where the amplitude specifies the normalized apodization profile and where ϕ_g is incorporated as the phase.

To apply this phase modulation to our FS writing scheme, the total grating phase is mapped to the physical distance between every laser-induced modification by:

$$\Delta x_n = \Lambda_g \left(1 - \frac{\phi_{\text{tot}}(n\Lambda_g) - \phi_{\text{tot}}((n-1)\Lambda_g)}{2\pi} \right), \quad (4)$$

$$\phi_{\text{tot}}(x) = \frac{2\pi x}{\Lambda_g} + \phi_g(x) + J_0^{-1}(|\kappa_n(x)|) \sin \left(\frac{2\pi x}{\Lambda_\phi} \right), \quad (5)$$

where Δx_n is the n^{th} spacing between the grating planes. A more visual interpretation of the process described above is presented in Fig. 7. which shows an example for a Gaussian apodization and an exaggerated linear chirp of 75 nm/mm. The modulation period was fixed at $\Lambda_\phi = 10 \mu\text{m}$. The target apodization $|\kappa_n(x)|$ and phase $\phi_g(x)$ profiles are presented in Fig. 7-A. $|\kappa_n(x)|$ is used to compute $A(x)$ using Eq. (3), and the modulation signal is shown in Fig. 7-(B). The distance between each grating planes is computed from Eq. (4) and (5), and is illustrated in Fig. 7-(C).

5.2. Arbitrary complex apodization profile

Combined with our high precision phase control strategy, the phase modulation apodization technique presented above allows the fabrication of arbitrary complex grating structures at very high spatial resolution, i.e. with very sharp phase and/or apodization change. To demonstrate our ability to write challenging apodized FBGs, we designed a structure that combines three

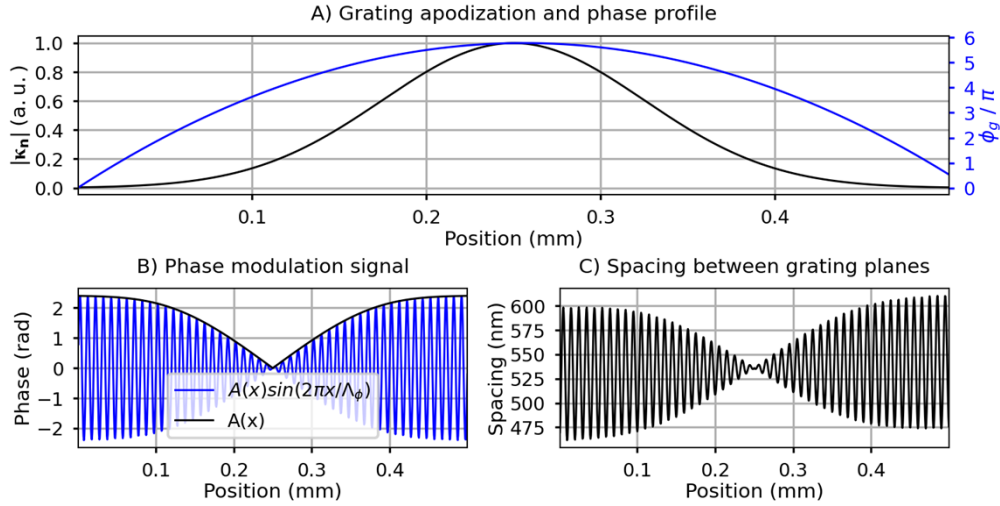


Fig. 7. A) Example of a Gaussian apodization profile and quadratic phase profile that produces a linear chirp. B) To achieve apodization, a phase modulated signal, represented by the blue curve, is added to the total phase of the grating. The black curve represents the modulation amplitude. The sinusoidal function has a modulation period $\Lambda_\phi = 10 \mu\text{m}$. C) Corresponding prescribed distance between each laser-inscribed modification as calculated by Eq. (4).

non-uniform FBGs typically used as a benchmark to show apodization performance, but all in a single structure written in a single pass. This includes a square-top FBG (sinc apodization), a linearly chirped Gaussian apodized (LCGA) FBG and a π phase-shifted distributed feedback (DFB) FBG, each centered at different Bragg wavelengths. The LCGA FBG is centered at $\lambda_B = 1568.7 \text{ nm}$ and has a chirp rate of 1 nm/mm . The DFB and sinc apodized FBGs are shifted by $\pm 20 \text{ nm}$, respectively. The maximum strength of the DFB was intentionally lowered to present a reflectivity spectrum with similar maximum reflectivity for the three sub-structures. Equation (6) and (7) represent the total apodization profile of this design and Eq. (8–10) are the apodization and phase functions of each sub-structure.

$$\kappa_n(x) = \exp(iK_0x) \left\{ \sum_{m=1}^3 |\kappa_{n,m}(x)| \exp(i(\Delta K_m x + \phi_{g,m}(x))) \right\} \quad (6)$$

$$\Delta K_m = -\frac{4\pi n_{\text{eff}}}{\lambda_B^2} \Delta \lambda_m \quad (7)$$

$$S = \text{sinc}\left(\frac{2\pi N_0}{L}(x - L/2)\right), \quad |\kappa_{n,1}(x)| = |S|, \quad \phi_{g,1}(x) = \pi \left(\frac{\text{sign}(S) + 1}{2}\right) \quad (8)$$

$$|\kappa_{n,2}(x)| = \exp\left(-\frac{1}{2}\left(\frac{x - L/2}{\sigma L/2}\right)^2\right), \quad \phi_{g,2}(x) = \frac{c}{2}x^2 \quad (9)$$

$$|\kappa_{n,3}(x)| = 0.12, \quad \phi_{g,3}(x) = \begin{cases} 0; & x < L/2 \\ \pi; & x \geq L/2 \end{cases} \quad (10)$$

where m is the sub-structure number, K_0 is the central wavevector given by $2\pi/\Lambda_g$, ΔK_m and $\Delta \lambda_m$ are the wavevector or wavelength offset, $|\kappa_{n,m}(x)|$ is the normalized apodization profile amplitude, $\phi_{g,m}$ is the grating phase, and L is the length. In the case of the LCGA structure, $\sigma = 0.3$,

$c = (K_{A_f} - K_{A_i})/L$. The parameter N_0 for the sinc apodized structure is $N_0 = 6$. The DFB has a π phase shift located in the middle of the grating.

Figure 8 shows the resulting complex normalized coupling coefficient $\kappa_n(x)$, calculated using Eq. (6) (6). Designing the FBG with a large bandwidth yields a structure with some high frequency features, where the amplitude and phase profile oscillate with a period as small as $20 \mu\text{m}$. The design proposed in Fig. 8 was inscribed at first order in an uncoated SMF-28 fiber using the methods described above. The FBG had a length of 10 mm, was written at $50 \mu\text{m/s}$ and a burst of 175 pulses per grating plane was chosen. The laser pulse energy was 275 nJ which corresponded to a maximum κ of about 525 m^{-1} . To resolve the small features, the period of the sinusoidal phase function was set to $\Lambda_\phi = 2.5 \mu\text{m}$.

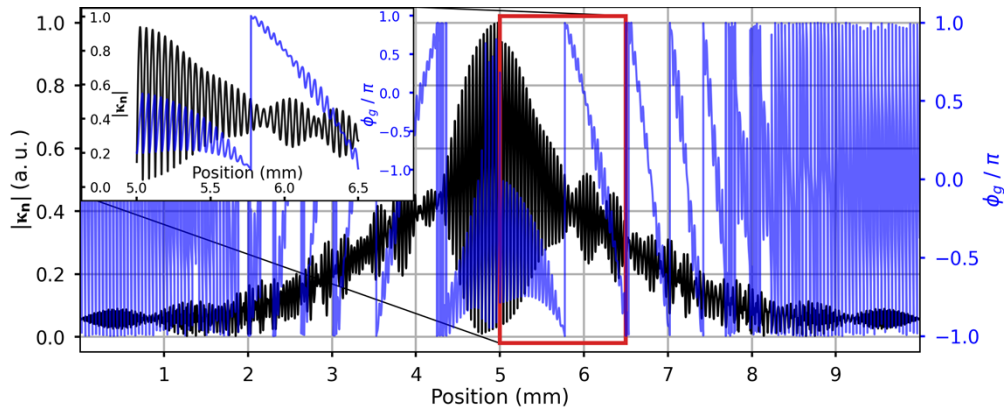


Fig. 8. Design of the apodization and phase profile used to demonstrate the ability to write arbitrary complex grating. The smallest feature has a periodicity of $20 \mu\text{m}$.

Figure 9 shows the reflection spectra of this FBG along with its numerical simulation. The simulation was performed using a simple thin-film method [46]. The typical features of the three FBG sub-structures, covering a bandwidth of 40 nm, are clearly distinguishable: The sinc function FBG shows a square response with 6 obvious oscillations (associated with $N_0 = 6$), the group delay of the LCGA FBG has a slope of -10.15 ps/nm , matching the designed chirp of 1 nm/mm , and the DFB resonant mode is well centered with the main Bragg resonance. The first side lobe levels of the sinc function and DFB gratings are respectively -16 dB and -12.5 dB , slightly higher than the predicted level. However, considering the complexity of the design and the good agreement between the numerical simulation and the fabricated FBG, this result proves the ability of the phase modulation method to perform apodization with high precision and high spatial resolution using a FS direct-writing method. It also shows that our phase control strategy based on PSO tracking is well adapted to precisely control the position of individual grating planes, even when their relative distance is aggressively modulated. The writing's imperfections are due to residual sources of noise such as high-frequency noise induced by the stage, vibrations, slight deviation from the core center, and laser power fluctuations. The effects of these can be observed as noisy and high-level side-bands straying from expected simulated profile.

It should be noted that this method of apodization is well adapted to any direct-writing scheme (PbP, LbL or PI-b-PI) where it is possible to control the exact position of each laser induced modification.

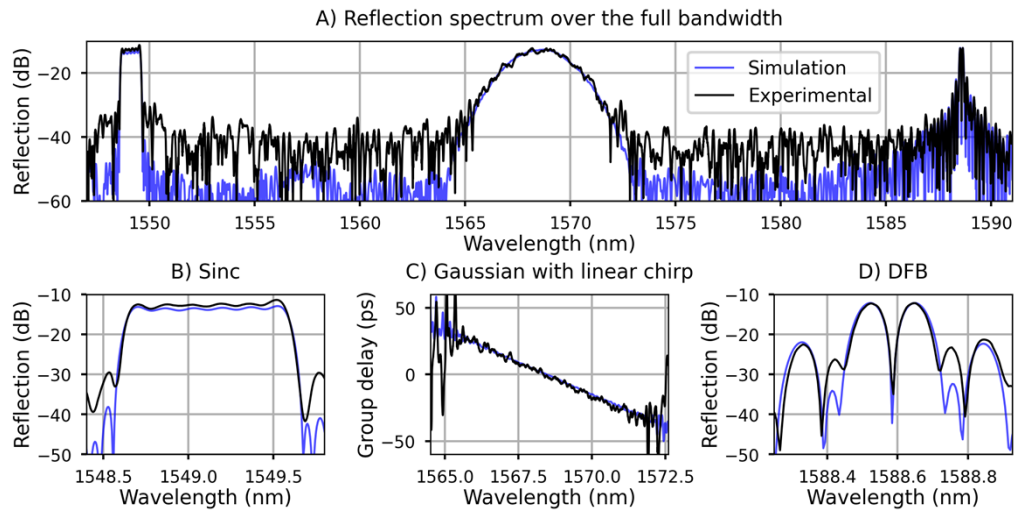


Fig. 9. Simulated vs. experimental reflection spectra of the complex-apodized FBG written in a single pass using the function described in Fig. 8. A) Broadband reflection spectrum. B) Zoom of the sinc function apodization response. C) Group delay of the linearly chirped and Gaussian apodized part. D) Zoom of the DFB response.

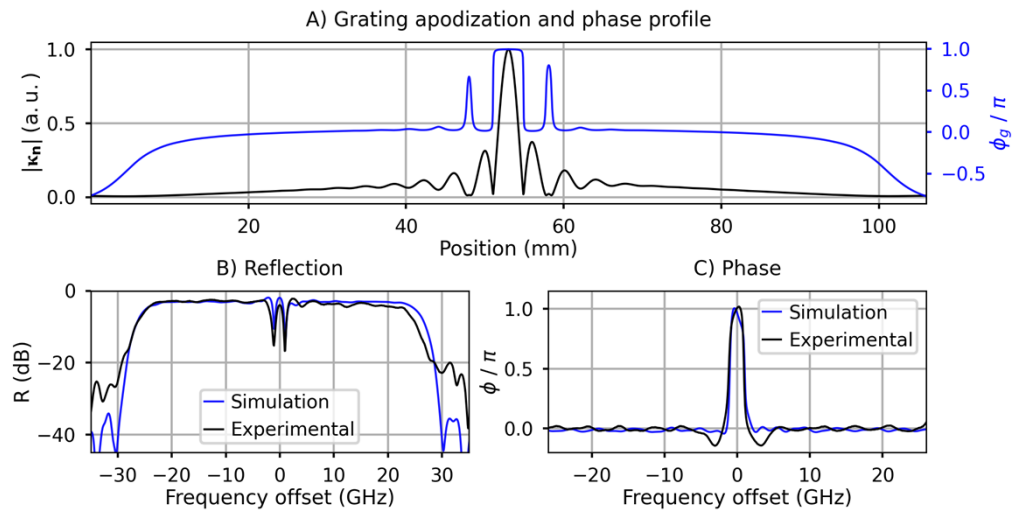


Fig. 10. A) Design of the grating apodization and phase profile of a 106 mm long FBG. B) and C) Simulated vs. measured reflection and phase response of the filter.

5.3. Complex ultra-long FBGs

To demonstrate the ability of our technique to maintain high quality over a longer distance, a phase-only filter, which requires a long FBG (>100 mm) to ensure a narrow spectral phase response, was designed [47] and successfully fabricated.

Figure 10-(A) shows the grating profile, which targets a square amplitude spectral response with a peak reflectivity of 50% and a bandwidth of 50 GHz. It is designed to impart a rectangular π phase shift to the central frequency of the main stopband, with a bandwidth of just 2 GHz. The FBG was written in an uncoated SMF-28, with a length of 106 mm, a target κ of 362 m^{-1} , and a modulation period of $\Lambda_\phi = 10 \text{ }\mu\text{m}$. Figure 10-(B) and C shows the simulated and measured spectral response (amplitude and phase) of this FBG. This result highlights the capacity of maintaining an excellent amplitude and phase control over a long distance, which is an essential requirement to achieve such narrow spectral phase response. The limitation toward even longer FBG may ultimately depends on the amplitude and phase error that can be tolerated.

6. Conclusion

This article proposed and demonstrated four different refinements that may be used together to enhance the capabilities for fabricating FBGs with direct-writing schemes based on FS lasers. Based on weak probe gratings measured by OFDR, a novel alignment procedure was implemented and successfully used to map the absolute core position of different types of fiber. This method is precise, flexible, and is non-destructive, i.e. a final strong and high-quality first order FBG can be written in the probed area. It can be seen as an alternative to the typical alignment method relying on an imaging system but requires the availability of an OFDR system. For the writing scheme itself, a phase control strategy based on PSO tracking was used to precisely control the position of each of the grating planes. It was also demonstrated that a multi-pulse approach provides a way to inscribe strong first-order grating with low insertion loss and high spectral quality. These writing methods made it possible to implement an apodization method based on phase modulation, allowing both phase and amplitude control within a few grating periods. This method of FS direct-writing can be used to fabricate long FBGs, with arbitrarily complex apodization and phase profiles, offering the potential for tailoring complex spectral functionalities over a large bandwidth. Our work now focuses on challenging applications that could not have been contemplated without our novel approach and which will be reported on in the future.

Funding. Natural Sciences and Engineering Research Council of Canada; Fonds de recherche du Québec – Nature et technologies; Canadian Foundation for Innovation.

Disclosures. The authors declare no conflicts of interest.

Data availability. Data underlying the results presented in this paper are not publicly available at this time but may be obtained from the authors upon reasonable request.

Supplemental document. See [Supplement 1](#) for supporting content.

References

1. J. He, B. Xu, X. Xu, C. Liao, and Y. Wang, "Review of Femtosecond-Laser-Inscribed Fiber Bragg Gratings: Fabrication Technologies and Sensing Applications," *Photonic Sens.* **11**(2), 203–226 (2021).
2. A. Martinez, I. Y. Khrushchev, and I. Bennion, "Direct inscription of Bragg gratings in coated fibers by an infrared femtosecond laser," *Opt. Lett.* **31**(11), 1603–1605 (2006).
3. A. V. Dostovalov, A. A. Wolf, A. V. Parygin, V. E. Zyubin, and S. A. Babin, "Femtosecond point-by-point inscription of Bragg gratings by drawing a coated fiber through ferrule," *Opt. Express* **24**(15), 16232–16237 (2016).
4. S. J. Mihailov, C. W. Smelser, P. Lu, R. B. Walker, D. Grobnic, H. Ding, G. Henderson, and J. Unruh, "Fiber bragg gratings made with a phase mask and 800-nm femtosecond radiation," *Opt. Lett.* **28**(12), 995–997 (2003).
5. A. Martinez, M. Dubov, I. Khrushchev, and I. Bennion, "Direct writing of fibre Bragg gratings by femtosecond laser," *Electron. Lett.* **40**(19), 1170 (2004).
6. P. Lu, S. J. Mihailov, H. Ding, D. Grobnic, R. B. Walker, D. Coulas, C. Hnatovsky, and A. Y. Naumov, "Plane-by-Plane Inscription of Grating Structures in Optical Fibers," *J. Lightwave Technol.* **36**(4), 926–931 (2018).

7. T. Osuch and Z. Jaroszewicz, "Numerical analysis of apodized fiber Bragg gratings formation using phase mask with variable diffraction efficiency," *Opt. Commun.* **284**(2), 567–572 (2011).
8. A. Rahman, K. Madhav, and M. M. Roth, "Complex phase masks for OH suppression filters in astronomy: part I: design," *Opt. Express* **28**(19), 27797–27807 (2020).
9. P. Roldan-Varona, D. Pallares-Aldeiturriaga, L. Rodriguez-Cobo, and J. M. Lopez-Higuera, "Slit Beam Shaping Technique for Femtosecond Laser Inscription of Enhanced Plane-by-Plane FBGs," *J. Lightwave Technol.* **38**(16), 4526–4532 (2020).
10. R. Kashyap, *Fiber Bragg Gratings* (Academic Press, 2010), Chap. 4.
11. K. Chah, D. Kinet, M. Wuilpart, P. Megret, and C. Caucheteur, "Femtosecond-laser-induced highly birefringent Bragg gratings in standard optical fiber," *Opt. Lett.* **38**(4), 594–596 (2013).
12. N. Jovanovic, J. Thomas, R. J. Williams, M. J. Steel, G. D. Marshall, A. Fuerbach, S. Nolte, A. Tunnermann, and M. J. Withford, "Polarization-dependent effects in point-by-point fiber Bragg gratings enable simple, linearly polarized fiber lasers," *Opt. Express* **17**(8), 6082–6095 (2009).
13. Y. Yu, J. Shi, F. Han, W. Sun, and X. Feng, "High-precision fiber Bragg gratings inscription by infrared femtosecond laser direct-writing method assisted with image recognition," *Opt. Express* **28**(6), 8937–8948 (2020).
14. G. D. Marshall, R. J. Williams, N. Jovanovic, M. J. Steel, and M. J. Withford, "Point-by-point written fiber-Bragg gratings and their application in complex grating designs," *Opt. Express* **18**(19), 19844–19859 (2010).
15. Q. Guo, Z. Zheng, B. Wang, X. Pan, S. Liu, Z. Tian, C. Chen, and Y. Yu, "Femtosecond Laser Fabricated Apodized Fiber Bragg Gratings Based on Energy Regulation," *Photonics* **8**(4), 110 (2021).
16. J. He, Z. Chen, X. Xu, J. He, B. Xu, B. Du, K. Guo, R. Chen, and Y. Wang, "Femtosecond laser line-by-line inscription of apodized fiber Bragg gratings," *Opt. Lett.* **46**(22), 5663–5666 (2021).
17. S. Antipov, M. Ams, R. J. Williams, E. Magi, M. J. Withford, and A. Fuerbach, "Direct infrared femtosecond laser inscription of chirped fiber Bragg gratings," *Opt. Express* **24**(1), 30–40 (2016).
18. T. A. Goebel, G. Bharathan, M. Ams, M. Heck, R. G. Kramer, C. Matzdorf, D. Richter, M. P. Siems, A. Fuerbach, and S. Nolte, "Realization of aperiodic fiber Bragg gratings with ultrashort laser pulses and the line-by-line technique," *Opt. Lett.* **43**(15), 3794–3797 (2018).
19. T. Geernaert, K. Kalli, C. Koutsides, M. Komodromos, T. Nasilowski, W. Urbanczyk, J. Wojcik, F. Berghmans, and H. Thienpont, "Point-by-point fiber Bragg grating inscription in free-standing step-index and photonic crystal fibers using near-IR femtosecond laser," *Opt. Lett.* **35**(10), 1647–1649 (2010).
20. Y. Lai, K. Zhou, K. Sugden, and I. Bennion, "Point-by-point inscription of first-order fiber Bragg grating for C-band applications," *Opt. Express* **15**(26), 18318–18325 (2007).
21. R. J. Williams, R. G. Kramer, S. Nolte, and M. J. Withford, "Femtosecond direct-writing of low-loss fiber Bragg gratings using a continuous core-scanning technique," *Opt. Lett.* **38**(11), 1918–1920 (2013).
22. P. S. Salter, M. J. Woolley, S. M. Morris, M. J. Booth, and J. A. J. Fells, "Femtosecond fiber Bragg grating fabrication with adaptive optics aberration compensation," *Opt. Lett.* **43**(24), 5993–5996 (2018).
23. R. Cheng and L. Chrostowski, "Apodization of Silicon Integrated Bragg Gratings Through Periodic Phase Modulation," *IEEE J. Sel. Top. Quantum Electron.* **26**(2), 1–15 (2020).
24. Aerotech, "Position Synchronized Output (PSO) – Coordinate Part Position with Process Control," retrieved November 19, 2021, <https://www.aerotech.com/position-synchronized-output-psy-coordinate-part-position-with-process-control/>.
25. D. Pallares-Aldeiturriaga, P. Roldan-Varona, L. Rodriguez-Cobo, and J. M. Lopez-Higuera, "Optical Fiber Sensors by Direct Laser Processing: A Review," *Sensors* **20**(23), 6971 (2020).
26. K. Zhou, M. Dubov, C. Mou, L. Zhang, V. K. Mezentsev, and I. Bennion, "Line-by-Line Fiber Bragg Grating Made by Femtosecond Laser," *IEEE Photonics Technol. Lett.* **22**(16), 1190–1192 (2010).
27. M. Gagne, S. Loranger, J. Lapointe, and R. Kashyap, "Fabrication of high quality, ultra-long fiber Bragg gratings: up to 2 million periods in phase," *Opt. Express* **22**(1), 387–398 (2014).
28. H. Zhang, S. M. Eaton, and P. R. Herman, "Single-step writing of Bragg grating waveguides in fused silica with an externally modulated femtosecond fiber laser," *Opt. Lett.* **32**(17), 2559–2561 (2007).
29. C. B. Schaffer, J. F. Garcia, and E. Mazur, "Bulk heating of transparent materials using a high-repetition-rate femtosecond laser," *Appl. Phys. A: Mater. Sci. Process.* **76**(3), 351–354 (2003).
30. M. Ams, P. Dekker, S. Gross, and M. J. Withford, "Fabricating waveguide Bragg gratings (WBGs) in bulk materials using ultrashort laser pulses," *Nanophotonics* **6**(5), 743–763 (2017).
31. R. Osellame, G. Cerullo, and R. Ramponi, *Femtosecond Laser Micromachining: Photonic and Microfluidic Devices in Transparent Materials* (Springer, 2012).
32. X. P. Pan, Q. Guo, Y. D. Wu, S. R. Liu, B. Wang, Y. S. Yu, and H. B. Sun, "Femtosecond laser inscribed chirped fiber Bragg gratings," *Opt. Lett.* **46**(9), 2059–2062 (2021).
33. Y. Zhang, Y. Zhu, D. Qiao, and P. Jiang, "Fiber Bragg gratings fabricated by femtosecond lasers for narrow-linewidth fiber laser," *Optik* **223**, 165451 (2020).
34. G. Bharathan, T. T. Fernandez, M. Ams, J. Y. Carree, S. Poulain, M. Poulain, and A. Fuerbach, "Femtosecond laser direct-written fiber Bragg gratings with high reflectivity and low loss at wavelengths beyond 4 microm," *Opt. Lett.* **45**(15), 4316–4319 (2020).
35. E. Ertorer, M. Haque, J. Li, and P. R. Herman, "Femtosecond laser filaments for rapid and flexible writing of fiber Bragg grating," *Opt. Express* **26**(7), 9323–9331 (2018).

36. LUNA, "Optical Backscatter Reflectometer 4600 : User Guide," (2006), retrieved May 18, 2022, <https://lunainc.com/product/obr-4600>.
37. R. J. Williams, R. G. Kramer, S. Nolte, M. J. Withford, and M. J. Steel, "Detuning in apodized point-by-point fiber Bragg gratings: insights into the grating morphology," *Opt. Express* **21**(22), 26854–26867 (2013).
38. T. Erdogan, "Fiber grating spectra," *J. Lightwave Technol.* **15**(8), 1277–1294 (1997).
39. Y. Chen, Y. Lai, and M. W. Cheong, "Distortion-free femtosecond laser inscription in free-standing optical fiber," *Appl. Opt.* **55**(21), 5575–5579 (2016).
40. R. Osellame, S. Taccheo, M. Marangoni, R. Ramponi, P. Laporta, D. Polli, S. De Silvestri, and G. Cerullo, "Femtosecond writing of active optical waveguides with astigmatically shaped beams," *J. Opt. Soc. Am. B* **20**(7), 1559 (2003).
41. X. Xu, J. He, J. He, B. Xu, R. Chen, K. Yang, C. Liao, Y. Yang, and Y. Wang, "Slit beam shaping for femtosecond laser point-by-point inscription of high-quality fiber Bragg gratings," *J. Lightwave Technol.* **39**(15), 5142–5148 (2021).
42. R. J. Williams, C. Voigtlander, G. D. Marshall, A. Tunnermann, S. Nolte, M. J. Steel, and M. J. Withford, "Point-by-point inscription of apodized fiber Bragg gratings," *Opt. Lett.* **36**(15), 2988–2990 (2011).
43. I. Ulyanov, D. V. Przhiiialkovskii, and O. V. Butov, "Point-by-point inscription of chirped apodized fiber Bragg gratings for application as ultrashort pulse stretchers," *Results Phys.* **32**, 105101 (2022).
44. S. Kaushal, R. Cheng, M. Ma, A. Mistry, M. Burla, L. Chrostowski, and J. Azaña, "Optical signal processing based on silicon photonics waveguide Bragg gratings: review," *Front. Optoelectron.* **11**(2), 163–188 (2018).
45. A. D. Simard, N. Belhadj, Y. Painchaud, and S. LaRochelle, "Apodized Silicon-on-Insulator Bragg Gratings," *IEEE Photonics Technol. Lett.* **24**(12), 1033–1035 (2012).
46. A. Mafi, "Anderson localization in a partially random Bragg grating and a conserved area theorem," *Opt. Lett.* **40**(15), 3603–3606 (2015).
47. S. Kaushal and J. Azaña, "Design of FBG-Based Linear Passive All-Optical NOT Gate," in *2019 Conference on Lasers and Electro-Optics Europe & European Quantum Electronics Conference (CLEO/Europe-EQEC)*, 2019), 1.